Separation of mono- and dibranched hydrocarbons on silicalite

4 AUTHORS, INCLUDING:

Elsa Jolimaître
IFP Energies nouvelles
22 PUBLICATIONS   461 CITATIONS

SEE PROFILE

K. Ragil
IFP Energies nouvelles
15 PUBLICATIONS   418 CITATIONS

SEE PROFILE

Melaz Tayakout-fayolle
Claude Bernard University Lyon 1
73 PUBLICATIONS   440 CITATIONS

SEE PROFILE

Separation of Mono- and Dibranched Hydrocarbons on Silicalite

E. Jolimaitre and K. Ragil

Institut Français du Pétrole, 92852 Rueil-Malmaison Cedex, France

M. Tayakout-Fayolle and C. Jallut

Laboratoire d'Automatique et de Génie des Procédés, Université Claude Bernard et ESCPE Lyon,
UMR 5007 CNRS, 43, 69622 Villeurbanne Cedex, France

Breakthrough curves for mixtures of C5 and C6 hydrocarbons with different degrees of branching were obtained experimentally on a silicalite molecular sieve by fixed-bed experiments. The kinetic separation of di- from monobranched hydrocarbons was feasible on this type of zeolite: dimethyl molecules enter silicalite crystals very slowly, whereas monomethyl molecules are quickly adsorbed. Experimental results were compared to a theoretical isothermal model, considering the variation of diffusivity with concentration according to the Maxwell–Stefan theory. The parameters of the model (adsorption equilibria and diffusivities) were determined from single-component breakthrough curves. Experimental curves were generally well represented by the model, but the variation of diffusivity with concentration, as predicted by the Maxwell–Stefan theory, did not significantly improve the model prediction of experimental breakthrough curves by using a mean value of diffusivity.

Introduction

Separation of doubled-branched paraffins from single-branched and normal paraffins is of great industrial interest, because of its potential applications in the enhancement of the octane number of fuel products. A potential separation technique would be an adsorption process based on the difference in the kinetics of diffusion between mono- and dibranched molecules. This is possible only if the pores of the adsorbent have a diameter close to the diameters of the molecules to be separated. In the case of C5–C6 paraffins, silicalite seems to be a good candidate.

Quite a few articles in the literature present the experimental estimation results of the adsorption isotherm and diffusion coefficients for C5–C6 paraffins in silicalite (Cavalcante and Ruthven, 1995a,b; Jolimaître et al., 2001; Millot, 1998; Millot et al., 1998; Post et al., 1994; Xiao and Wei, 1992). However, the discrepancy between the different experimental results is sometimes very important, particularly concerning diffusivities, which can vary in more than three orders of magnitude, depending on the study. This problem is

not linked to the nature of the paraffins–silicalite system, but has been very well known for a long time to the specialists of adsorption. Kärger and Ruthven (1981, 1989) have reviewed the subject and proposed an explanation based on the difference in time constants between the experimental techniques, yet a great many questions still remain. As a consequence, it is very risky to insert literature data directly into a model of the process. These data are more useful as a qualitative result for predicting the potentiality of a zeolite for a given kinetic separation.

For the time being, only a complete study (parameter estimation and simulation) with the same model and the same adsorbent seems to be really reliable. Farooq et al. (1993), Farooq and Ruthven (1991), and Van der Broeke and Krishna (1995) have all successfully applied the same principle: parameters are estimated from single-component breakthrough curves and inserted into the model to simulate the more complicated multicomponent curves. In all these studies, a comparison is made between two diffusion models: the classic Fick model with constant diffusivities and the Maxwell–Stefan model, that supposes a variation in the dif-

fusivities with the adsorbed-phase concentration of all components. The conclusion is always the same: the Maxwell–Stefan approach allows a better representation of the experimental results than the constant diffusivity approach.

The aim of this work is, therefore, to study the dynamics of adsorption and diffusion of three paraffins in silicalite, in order to evaluate the separation feasibility. The chosen molecules are isopentane (iP), 2-methylpentane (2MP), and 2,2-dimethylbutane (22DMB). Experimental breakthrough curves were obtained using a pilot plant adsorption column. A model has been developed that is used, on the one hand, to estimate adsorption and diffusion parameters from single-component curves, and on the other hand, to simulate the multicomponent breakthrough curves. Comparing experimental and simulated breakthrough curves allows us to validate (or to invalidate) different assumptions concerning the diffusion phenomena inside the pores of the zeolite.

To design a separation process, the model, which is used in this study just for simulating breakthrough curves, will have to be integrated in a more global process model [pressure swing adsorption (PSA) or simulated moving bed (SMB)], with the objective of estimating the productivities and the purities for a given kinetic separation. To obtain precise and reliable results, it is very clear that the representation of diffusion in the model has to be the best possible. But PSA and SMB models require many iterations to reach the steady state, and the simplest and fastest model is, therefore, recommended to limit calculation costs.

Our results lead to a compromise between these two options: a constant-diffusivity model can be sufficient if a mean value of the diffusivity (taking into account the mean value of the adsorbed concentration) is used.

Description of the Model

Model assumptions

1. The flow pattern is described by the axial dispersed plug-flow model. Axial dispersion, which is usually negligible in industrial units, is taken into account in our model, because of the small size of the column and the small interstitial velocity.

2. The column is an isotherm. This assumption is not fully respected when the adsorbed quantities are important. However, taking the temperature variations in the column into account would greatly complicate the model, and the uncertainties from the poor knowledge of the thermal parameters would certainly be even greater. Moreover, the column has a small diameter, and it is placed in a heated oven for temperature regulation. As a result, a maximum rise of 8°C was observed experimentally.

3. Frictional pressure drop through the column is negligible.

4. The ideal gas law applies.

5. The variation of fluid velocity along the column length, as determined by the global mass balance, is accounted for.

6. The adsorption equilibrium is represented by the generalized Langmuir model, with the same adsorption capacities for all adsorbates. This assumption is based on results in the literature, which show that a maximum of four molecules of isopentane, 2MP, and 22DMB can enter the silicalite cells.

7. An external film resistance between the fluid and the particle surface is assumed. In practice, this resistance was found to be negligible in our experimental conditions. It was nevertheless kept in the model, for numerical considerations.

8. The adsorbent has a bidisperse pore structure. The silicalite crystals used in this study have a mean radius of 2 μm. To minimize the pressure drop, these crystals were agglomerated to form particles. The adsorbent introduced into the column was therefore bidisperse, and macropore diffusional resistance was taken into account in the model. However, since the micropore resistance is supposed to be controlling in a kinetic separation, a complete description of macropore diffusion did not seem to be necessary. The macropore resistance is therefore lumped: concentration in the macropore is assumed to be uniform, and an additional mass-transfer coefficient, k_t, is introduced at the surface of the crystals.

9. The gradient of chemical potential is assumed to be the driving force for diffusion in the zeolite lattice. The countercurrent diffusion coefficients are assumed to be negligible. The diffusivity of a given adsorbate depends on the adsorbed-phase concentration of each compound through the thermodynamic adsorption equilibria.

Equations

The preceding hypotheses lead to the following set of equations

Fluid Phase.

$$\frac{\partial \hat{C}}{\partial t} = D_L \cdot \frac{\partial^2 \hat{C}}{\partial z^2} - \frac{\partial v \cdot \hat{C}}{\partial z} - \left(\frac{1 - \epsilon_i}{\epsilon_i} \right) \cdot \frac{3}{R_p} \cdot k_p \cdot \left(\hat{C} - \hat{C}_p \right) \quad (1)$$

$$\frac{\partial v \cdot \hat{C}}{\partial z} = v \cdot \frac{\partial \hat{C}}{\partial z} + \hat{C} \cdot \frac{\partial v}{\partial z} \quad (2)$$

Boundary conditions

$$\left. \frac{\partial \hat{C}}{\partial z} \right|_{z=L} = 0 \quad (3)$$

$$D_L \cdot \left. \frac{\partial \hat{C}}{\partial z} \right|_{z=0} = -v_0 \cdot \left(\hat{C} \big|_{z=0-} - \hat{C} \big|_{z=0+} \right) \quad (4)$$

Velocity variation

$$C_T \cdot \frac{\partial v}{\partial z} = -\frac{1 - \epsilon_i}{\epsilon_i} \cdot \frac{3 \cdot \epsilon_p \cdot k_p}{R_p} \cdot \sum_{j=1}^{N} \left(C_j - C_{pj} \right) \quad (5)$$

Macropore Mass Balance.

$$\frac{\partial \hat{C}_p}{\partial t} = \frac{3 \cdot k_p}{R_p \cdot \epsilon_p} \cdot \left(\hat{C} - \hat{C}_p \right) - \left(\frac{1 - \epsilon_p}{\epsilon_p} \right)$$

$$\cdot \frac{3}{R_c} \cdot [k_t] \cdot \left(\hat{C} - \hat{C}_p \big|_{r_c = R_c} \right) \quad (6)$$

$$[k_t] = \begin{bmatrix} k_{t1} & & 0 \\ & k_{t2} & \\ 0 & & k_{t3} \end{bmatrix} \quad (7)$$

Crystal Mass Balance.

$$\frac{\partial \hat{q}}{\partial t} = \frac{1}{r_c^2} \cdot \frac{\partial}{\partial r_c}\left(r_c^2 \cdot [D] \cdot \frac{\partial \hat{q}}{\partial r_c}\right) \quad (8)$$

$$[D] = \begin{bmatrix} D_{c1} & 0 & 0 \\ 0 & D_{c2} & 0 \\ 0 & 0 & D_{c3} \end{bmatrix}$$

$$= \frac{1}{1-\theta_t} \cdot \begin{bmatrix} D_1 & 0 & 0 \\ 0 & D_2 & 0 \\ 0 & 0 & D_3 \end{bmatrix}$$

$$\cdot \begin{bmatrix} 1-\theta_2-\theta_3 & \theta_1 & \theta_1 \\ \theta_2 & 1-\theta_1-\theta_3 & \theta_2 \\ \theta_3 & \theta_3 & 1-\theta_1-\theta_2 \end{bmatrix} \quad (9)$$

Boundary conditions

$$\left.\frac{\partial \hat{q}}{\partial r_c}\right|_{r_c = 0} = 0 \quad (10)$$

$$[D_c] \cdot \left.\frac{\partial \hat{q}}{\partial r_c}\right|_{r_c = R_c} = [k_t] \cdot \left(\hat{C}_p - \hat{C}_p\big|_{r_c = R_c}\right) \quad (11)$$

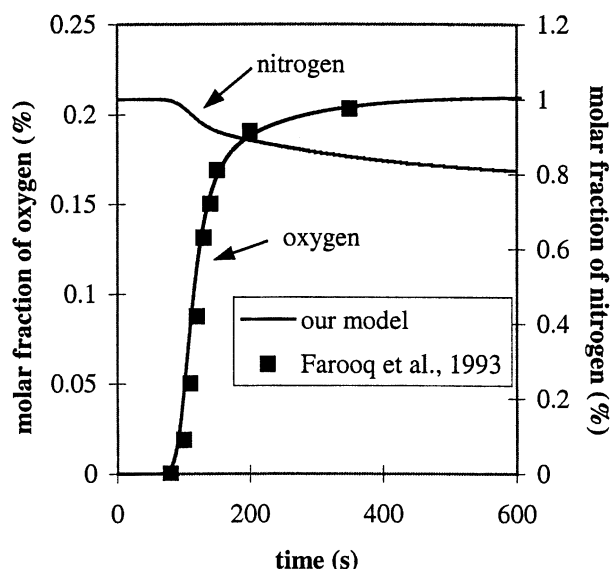*Thermodynamical Equilibrium Conditions.*

$$C_{pj}\big|_{r_c = R_c} = b_j^{-1} \cdot \frac{q_j\big|_{r_c = R_c}}{q_s - \sum_{1=1}^{n_c} q_1\big|_{r_c = R_c}} \quad (12)$$

Method of solution

Equations 1 to 12 were written in the collocation form, thus, reducing the set of partial differential equations to a set of algebraic and ordinary differential equations. These equations were then numerically integrated using the IMSL DASPG routine, based on Petzold-Gear's integration method. Fifteen to 25 interval points were needed along the length of the bed, depending on the stiffness of the solution, and 5 points were needed along the crystal radius.

Model validation

The model was validated by comparison with the results in the literature. The model of Farooq et al. (1993) was chosen. This model, used by the authors to simulate the O_2/N_2 sepa-

Table 1. Validation of the Model: Values of Parameters

Parameters	Values
ϵ_i	0.5
R_c (m)	3×10^{-3}
D_c (m²/s)	3×10^{-11}
k_t (m/s)	10^{-3}
L (m)	0.1
v (m/s)	10^{-3}
K	4×10^4
Pe	0.8, 5, and 100

Figure 1. Simulations with our model vs. simulations with Farooq et al. (1993) in the same conditions.

ration, is similar to ours, except that it is monodisperse. Simulations were therefore made by imposing $\epsilon_p = 0$ and $k_p \rightarrow \infty$. The values of the other parameters are the same as those of Farooq et al. (1993), and are given in Table 1. Comparisons between the simulations made by Farooq et al. (1993) and with our model are shown in Figure 1. As expected, the two models have very similar results. This allows us to confirm the validity of our model.

Experimental Section

Adsorbent characterization

The silicalite crystals used in this study all come from the same sample, supplied by Zeolist International. Its Si/Al ratio measured by X fluorescence is $500 \pm 50\%$. The mean crystal diameter is $R_c = 2 \times 10^{-6}$ m.

Particles were made at the Institut Français du Pétrole using extrusion with a binder (silica). Extrudates are small cylinders with a diameter of 1 mm and a mean length of 4 mm. To simplify the model, particles were supposed to be spherical, with the mean radius being the radius of the sphere having the same surface as the particle

$$R_p = \sqrt{\frac{d_p \cdot L_p}{4}} \approx 1 \text{ mm} \quad (13)$$

where R_p is the calculated mean radius of the particles, d_p and L_p are, respectively, the diameter and the mean length of the extrudates. Two different extrudates made with the same silicalite were used in this study. Their properties are listed in Table 2

$$t = \frac{\text{Mass of binder}}{\text{Mass of particle}} \quad (14)$$

The ratio of the binder present in the particle (Eq. 14) was determined by gravimetric uptake measurements, by compar-

ing the quantity of 3-methylpentane adsorbed in crystals and in particles, for three different temperatures. Activation of the adsorbent was performed by raising the temperature to 450°C for 4 h.

Experimental setup

A stainless-steel column ($L = 79.8$ cm and $d_c = 1.6$ cm) is filled with the adsorbent particles and placed into an oven. A mixture of nitrogen and hydrocarbons is injected at the bottom of the column. Nitrogen flow is regulated by a mass flowmeter. The hydrocarbon liquid mixture is pumped with an ISCO pump (0–500 mL/h) and vaporized by passing it through an oven heated to 300°C before it enters the column. At the output of the column, a fixed flow of nitrogen, controlled by a mass flowmeter, is added to the outlet in order to prevent condensation. The flow then passes through a pressure regulator to eliminate any pressure fluctuation when the fluid velocity inside the column changes due to adsorption and desorption phenomena.

Analysis of the fluid composition is made with a HP 5890 series II chromatograph. When only one hydrocarbon is present in the charge, a small percentage of the flow is directed to a FID detector in order to obtain a continuous output signal. For binary and ternary breakthrough curves, the output flow is sampled at predefined time intervals during the experiment and analyzed by chromatography afterwards. A constant and predetermined propane flow is added to the flow before sampling. The flow rate of each component is, therefore, determined by comparing the quantity of this component in the sample to that of propane.

At the end of each experiment, the adsorbent is regenerated by passing pure nitrogen through the column and raising the temperature up to 350°C for 3 h.

Results and Discussion

Parameter estimation

Method. Pure-component isotherms and self-diffusion coefficients were estimated from single-component breakthrough curves, using the model presented earlier. All parameters of the model were fixed except for the Langmuir coefficient, b, and the self-diffusion coefficient, D. In particular, the quantity adsorbed at saturation into the silicalite was fixed at the theoretical value of 4 molecules/cell (1,240

Table 2. Properties of the Extrudates

	Extrudates No. 1	Extrudates No. 2
ϵ_p	0.35	0.44
ϵ_i	0.33	0.4
t	0.44	0.38
q_s (mol/m^3)	693.8	771.3

mol/m^3 of silicalite). The estimation procedure then consists of finding b and D for 2MP, 22DMB, and iP, so as to minimize the difference between the experimental and simulated breakthrough curves. The optimized value of the Langmuir parameter b is used to calculate the quantity adsorbed into the zeolite at the given temperature and hydrocarbon concentration using the Langmuir equation for a single adsorbed component:

$$q = q_s \cdot \frac{b \cdot C}{1 + b \cdot C}. \qquad (15)$$

Hence, estimation of the parameter b for different fluid concentrations allows the pure component isotherms to be determined.
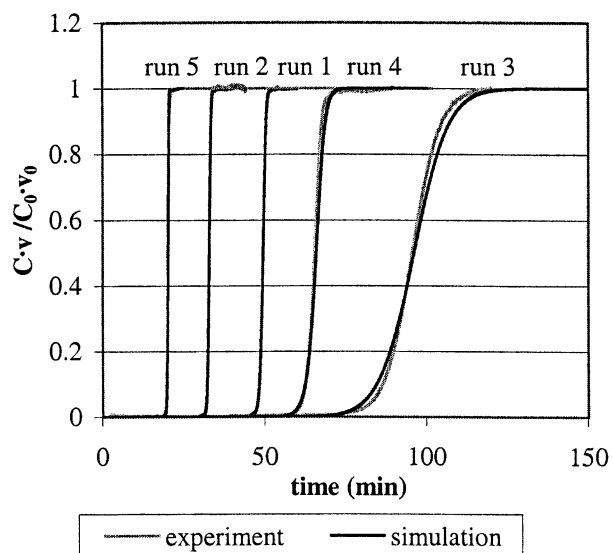
Experimental conditions of the single-component breakthrough curves for 2MP, iP, and 22DMB are given in Table 3. The corresponding experimental and simulated breakthrough curves for 2MP and 22DMB are plotted in Figures 2 and 3 (the curves for iP and 2MP are very similar, so the curves for iP are not shown). The model is a good representation of the experimental curves: simulations are so close to experimental results that they are difficult to distinguish.

Equilibrium Results. The adsorption isotherms for 2MP, 22DMB, and iP on silicalite at 200°C, as determined by the previously mentioned method, are plotted in Figures 4, 5, and 6. These figures also show results from the literature for the same systems and the Langmuir plots of our experimental results. Several remarks can be made concerning the isotherms:

1. Our results are in good agreement with those in the literature, except for 22DMB, for which the data scattering is very important. This may be due to the fact that 22DMB has a kinetic diameter very close to the channel's aperture. The diffusivity of this molecule in silicalite is, therefore, very slow, which can lead to important experimental errors. Further-

Table 3. Experimental Conditions for Single-Component Breakthrough Curves

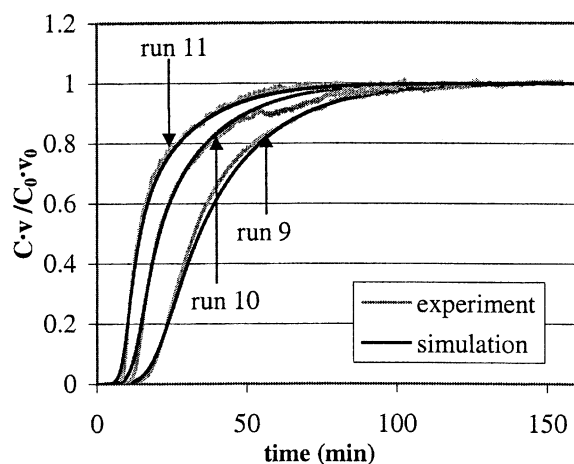| Run	Extrudates	Total Con. (mol/m^3)	Conc. in Hydroc. (mol/m^3)	Inlet Inters. Vel. (m/s)	Total Press. (Pa)	Hydroc. Studied
1	1	127	3.83	4.12×10^{-2}	5×10^5	2MP
2	1	254	7.65	4.12×10^{-2}	10×10^5	2MP
3	2	127	0.38	3.15×10^{-2}	5×10^5	2MP
4	2	127	1.52	3.18×10^{-2}	5×10^5	2MP
5	2	381	11.50	3.14×10^{-2}	15×10^5	2MP
6	1	127	4.24	4.20×10^{-2}	5×10^5	iP
7	1	254	8.47	4.14×10^{-2}	10×10^5	iP
8	1	381	12.71	4.14×10^{-2}	15×10^5	iP
9	1	127	3.77	4.12×10^{-2}	5×10^5	22DMB
10	1	254	7.53	4.12×10^{-2}	10×10^5	22DMB
11	1	381	11.30	4.12×10^{-2}	15×10^5	22DMB

Figure 2. Experimental vs. simulated breakthrough curves for 2MP.

The corresponding experimental conditions are given in Table 3, and the equilibrium and kinetic values in Table 4.

Figure 3. Experimental vs. simulated breakthrough curves for 22DMB.
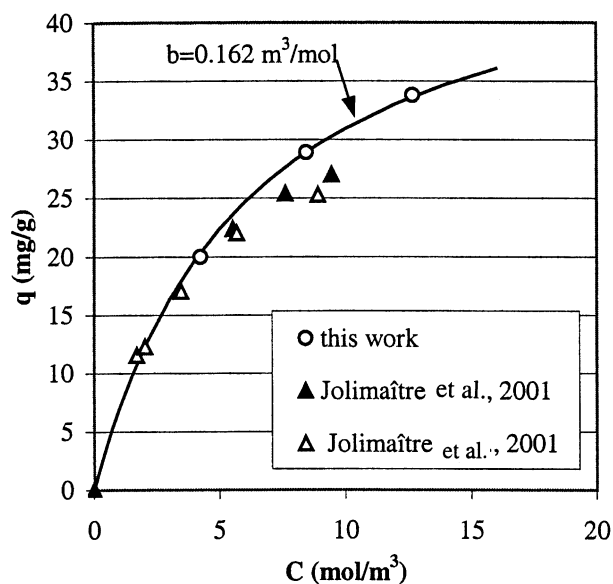
The corresponding experimental conditions are given in Table 3, and the equilibrium and kinetic values in Table 4.
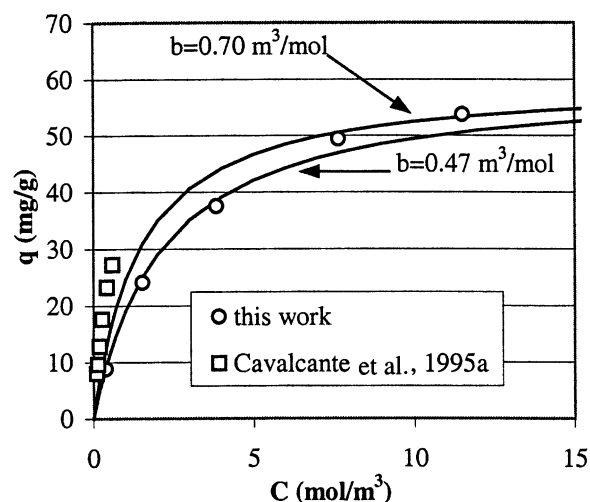
Figure 4. Comparison of adsorption isotherms of 2-methylpentane in silicalite at 200°C.
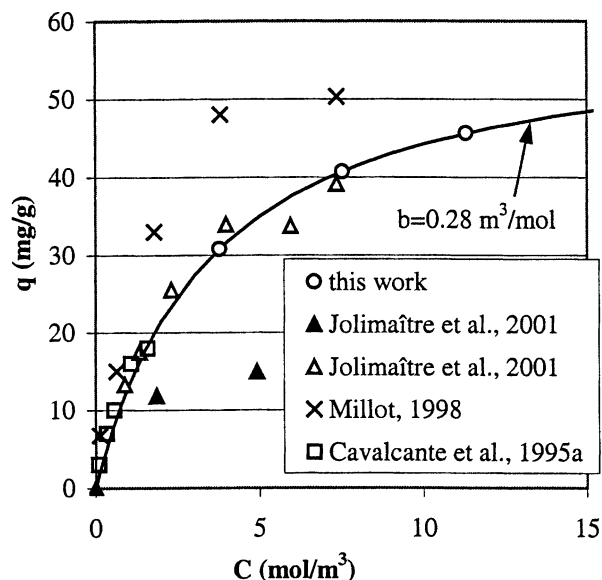

Figure 5. Comparison of adsorption isotherms of isopentane in silicalite at 200°C.

The results of Jolimaitre et al. are classified as follows: (1) chromatographic data; (2) uptake data.

more, a small change in the adsorbent structure or chemical composition could have a greater effect on 22DMB than on the smaller hydrocarbon molecules.

2. Our equilibrium data are not in agreement with the work of Cavalcante et al. (1995a). This disagreement was cited in a previous study (Jolimaître et al., 2001) and is confirmed here: at a given concentration, quantities adsorbed in silicalite as measured by Cavalcante et al. (1995a) are always higher than our data.

3. The isotherms of iP and 22DMB can be well represented by the Langmuir model, with the quantity adsorbed at saturation, q_s, fixed at the theoretical value of 4 molecules per cell (1240 mol/m^3 of silicalite). However, as shown in

Figure 4, the 2MP isotherm cannot be modeled with these hypotheses: experimental points lie between two Langmuir curves ($b = 0.5$ and $b = 0.7$ m^3/mol). Of course, it would be possible to correctly represent the isotherm by allowing a change in the q_s value, but this would conflict with the hypothesis of our model that all three products have the same adsorption capacity. This points out one of the limits of this model, which should be corrected in the future. For the rest of this study, the 2MP isotherm was modeled with $b = 0.5$ m^3/mol.

Self-Diffusivities. The values of the estimated self-diffusion coefficients, D, of 2MP, iP, and 22DMB can be found in Table 4. The self-diffusivity of iP and 22DMB is the same for all

Figure 6. Comparison of adsorption isotherms of 2,2-dimethylbutane in silicalite at 200°C.

Results of Jolimaitre et al. are classified as follows: (1) chromatographic data; (2) uptake data.

experiments, which means that no variation with concentration is observed. For 2MP, the data are more scattered, but no real trend can be found. As previously mentioned, it was necessary to use a different Langmuir coefficient, b, in order to represent the 2MP breakthrough curves. It is very probable that the variations of the estimated 2MP self-diffusivity are linked to the variations of the Langmuir coefficient. Indeed, the effective diffusivity depends on the adsorption equilibrium through the Maxwell–Stefan equation (that is to say, the Darken equation in the single adsorbed component case). The general tendency is the expected one: $D(iP) > D(2MP) > D(22DMB)$. The diffusivities of iP and 2MP are very close, whereas the diffusivity of 22DMB is about two orders of magnitude smaller. The self-diffusion coefficients at 200°C in the literature are compared to our values in Table 5. Concerning 22DMB, the data are all at the same order of

Table 4. Langmuir Coefficient b and Self-Diffusivity D from Single-Component Breakthrough Curves*

Run	b (m^3/mol)	D (m^2/s)	q (mg/g) Calc. from Eq. 15	Hydroc. Studied
1	0.435	2×10^{-14}	37.5	2MP
2	0.61	8×10^{-15}	49.4	2MP
3	0.45	2.5×10^{-14}	8.8	2MP
4	0.44	2.5×10^{-14}	24.1	2MP
5	0.75	1.4×10^{-14}	53.8	2MP
6	0.157	3×10^{-14}	20.0	iP
7	0.162	3×10^{-14}	28.9	iP
8	0.164	3×10^{-14}	33.8	iP
9	0.28	2.5×10^{-16}	30.8	22DMB
10	0.28	2.5×10^{-16}	40.7	22DMB
11	0.28	2.5×10^{-16}	45.6	22DMB

*Quantity adsorbed q is calculated using the estimated value of b and the theoretical value of q_s.

Table 5. Self-Diffusion Coefficients at 200°C, Comparison with Other Studies

	Reference	Exp. Technique	D (m^2/s)
iP	This study	Breakthrough curves	3×10^{-14}
	Jolimaître et al., 2001	Chrom.	4.9×10^{-15}
	Xiao & Wei, 1992	Uptake	1.1×10^{-11}
2MP	This study	Breakthrough Curves	2.0×10^{-14}
	Cavalcante & Ruthven, 1995b	Uptake	8.0×10^{-12}
22DMB	This study	Breakthrough Curves	2.5×10^{-16}
	Jolimaître et al., 2001	Chrom.	2.63×10^{-16}
	Xiao & Wei, 1992	Uptake	2.0×10^{-15}
	Cavalcante & Ruthven, 1995b	Uptake	8.2×10^{-15}
	Post et al., 1984	Chrom.	6.3×10^{-17}

magnitude, that is, between 6×10^{-17} and 8×10^{-15} m^2/s, which is very similar to the diffusivity data obtained by different experimental techniques. Our value is equal to the average of these data. Concerning 2MP and iP, the diffusivities measured in this study are lower than the few results cited in the literature. This confirms that it is very risky to directly use the diffusion data found in the literature.

Simulation of multicomponent breakthrough curves

Multicomponent breakthrough curves have been simulated using the estimated values of the isotherms and of the self-diffusion coefficients given in Table 4. Porosities and adsorption capacities are given in Table 2, and the experimental conditions of the multicomponent experiments in Table 6. Axial dispersion coefficient D_L was evaluated using the equation (Ruthven, 1984)

$$D_L = \gamma_1 \cdot D_m + \gamma_2 \cdot 2 \cdot R_p \cdot v \quad (16)$$

with

$$\gamma_1 = 0.45 + 0.55 \cdot \epsilon_i$$
$$\gamma_2 = 0.5$$

Table 6. Experimental Conditions for Multicomponent Breakthrough Curves*

Run	Extruduates	$C_0(iP)$ (mol/m^3)	$C_0(2MP)$ (mol/m^3)	$C_0(22DMB)$ (mol/m^3)	v (cm/s)
12	2	6.27	6.60	0	1.97
13	2	5.50	0	7.00	1.97
14	1	5.50	0	7.00	2.62
15	2	42.04	0	53.51	1.96
16	1	42.04	0	53.51	2.63
17	2	0	5.76	6.76	1.90
18	2	0	43.77	51.38	1.88
19	2	5.51	12.04	7.24	1.97
20	2	20.60	44.98	27.04	1.98
21	2	9.54	12.80	3.02	1.97
22	2	36.24	44.83	11.73	1.92

*Temperature and pressure conditions are fixed at 200°C and 5 bar.

Particle film resistance was calculated using the correlation of Wakao and Funazkri (1978)

$$Sh = 2 + 1.1 \cdot Sc^{1/3} \cdot Re^{0.6} \qquad (17)$$

where Sh is the Sherwood number $Sh = (2 \cdot k_p \cdot R_p)/D_m$, Sc is the Schmidt number $Sc = \mu_f/(\rho_f \cdot D_m)$, and Re is the Reynolds number $Re = [\rho_f \cdot v \cdot \epsilon_i \cdot (2 \cdot R_p)]/\mu_f$.

Particle film resistance is always negligible in our experimental conditions, but it was kept in the model equations for numerical reasons. It smoothens the concentration gradient around the particle, and, thus, facilitates the convergence of the algorithm.

Crystal film resistance coefficient k_t was evaluated by assuming that the contribution of k_t to the overall mass-transfer resistance is the same as that of the macropore when moment analysis is used (Ruthven, 1984)

$$k_t = \frac{15 \cdot D_p \cdot \epsilon_p \cdot R_c}{3 \cdot R_p^2} \qquad (18)$$

This method was already successfully applied in the work of Jolimaitre et al. (2001). The determination of D_p is possible using the classic relation (Ruthven, 1984)

$$\frac{1}{D_T} = \frac{1}{D_K} + \frac{1}{D_m} \qquad (19)$$

with

$$D_p = \frac{D_T}{\tau} \qquad (20)$$

Knudsen diffusivity is estimated using the following theoretical relation (Ruthven, 1984)

$$D_K = 9{,}700 \cdot r_{\text{pore}} \cdot \left(\frac{T}{M}\right)^{1/2} \qquad (21)$$

Molecular diffusivity, D_m, is calculated with the Chapman−Enskog equation (Reid et al., 1987). Knudsen diffusivity and molecular diffusivity in nitrogen are assumed to be the same for the three hydrocarbon molecules, and not to depend on the gas-phase concentration. Molecular weight for calculating Knudsen diffusivity is taken to be 86 g/mol. This is not true for iP, but the resulting error is neglected.

Using these correlations, all the parameters of the model are known, and simulations of the experimental breakthrough curves can be made.

Before simulating all the breakthrough curves, it is interesting to study the influence on the model performance of two of the model assumptions: the variations with concentration of the effective diffusivity by the Maxwell−Stefan theory, and the variation of fluid velocity along the length of the column. The objective is to find the simplest version of the model that can still correctly represent the experimental results. In other words, we wish to find the model that is best adapted to the present experimental conditions.

Influence of the Diffusion Model. Three different diffusion models were compared.

Model 1. The model based on the Maxwell−Stefan theory with no countercurrent diffusion, which was presented in the

first part of this article. At any time, effective diffusivities depend on the adsorbed concentrations of all components. It is the more general model.

Model 2. A simplified model, with constant effective diffusivities. Variation of diffusivity with concentration is still taken into account by the Darken equation in the following way

$$D_{cj} = \frac{D_j}{1 - \dfrac{\theta_{j,\text{final}}}{2}} \qquad (22)$$

where $\theta_{j,\text{final}}$ is the adsorbed fraction of j at equilibrium with the inlet gas concentration

$$\theta_{j,\text{final}} = \frac{b_j \cdot C_{0j}}{1 + \sum\limits_{i=1}^{nc} b_i \cdot C_{0i}} \qquad (23)$$

In this second model, diffusion coefficients are constant for a given experiment, but vary from one experiment to another, depending on the inlet concentration of each of the compounds.

Model 3. An even simpler model, with constant diffusivities equal to the values of the self-diffusivities. Diffusion coefficients are then constant for all experiments.

The expression of the effective diffusivity matrix $[D]$ for the three models is given in Table 7.

Comparisons of the three models for run 17 are given in Figure 7. Model 1 seems to better represent the breakthrough time for both 2MP and 22DMB, whereas models 2 and 3 better predict the roll-up amplitude. As expected, model 2 is halfway between model 1 (instantaneous variation of diffusivity with adsorbed phase concentration) and model 3 (constant self-diffusivity). The more adapted model has, therefore, to be chosen between model 1 and 2. To make this choice, two other runs (runs 12 and 13) were simulated with model 1 and model 2. Results are given on Figures 8 and 9. In run 12 (Figure 9), no real difference can be seen between the two models. Diffusivity variation with concentration is

Table 7. Effective Diffusivity Matrix for the Three Diffusion Models Studied

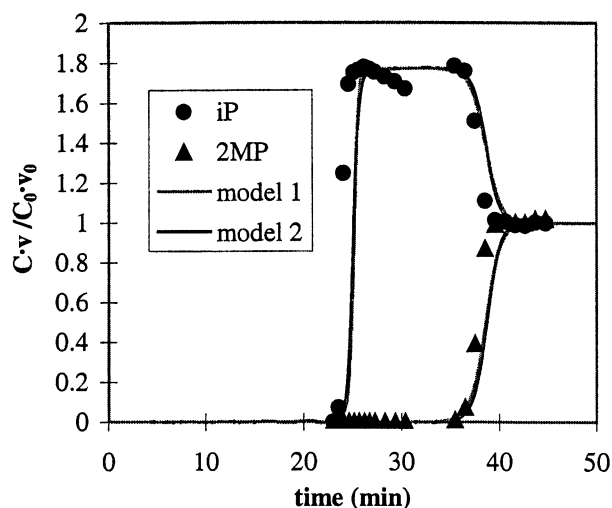| Model	Diffusivity Matrix
1	$[D_c] = \dfrac{1}{1 - \theta_t} \cdot \begin{bmatrix} D_1 & 0 & 0 \\ 0 & D_2 & 0 \\ 0 & 0 & D_3 \end{bmatrix}$ $\begin{bmatrix} 1 - \theta_2 - \theta_3 & \theta_1 & \theta_1 \\ \theta_2 & 1 - \theta_1 - \theta_3 & \theta_2 \\ \theta_3 & \theta_3 & 1 - \theta_1 - \theta_2 \end{bmatrix}$
2	$[D_c] = \begin{bmatrix} D_{c1} & 0 & 0 \\ 0 & D_{c2} & 0 \\ 0 & 0 & D_{c3} \end{bmatrix}$
3	$[D_c] = \begin{bmatrix} D_1 & 0 & 0 \\ 0 & D_2 & 0 \\ 0 & 0 & D_3 \end{bmatrix}$
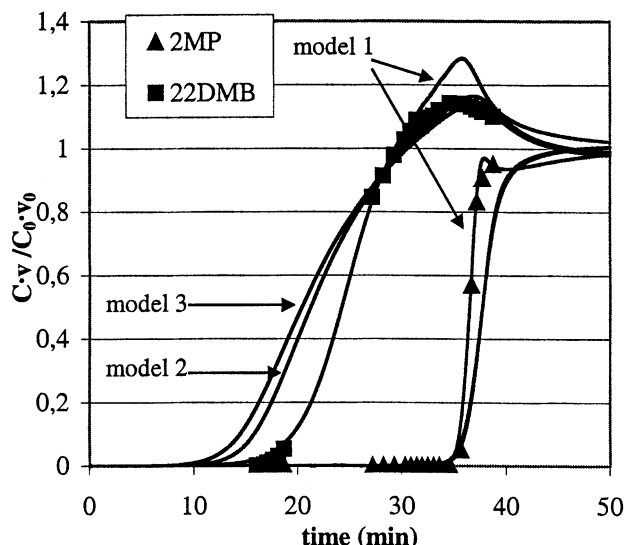
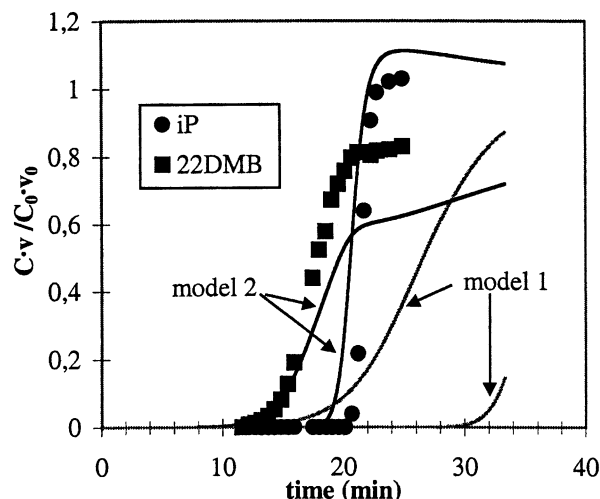**Figure 7. Simulations of run 17 with different hypotheses.**

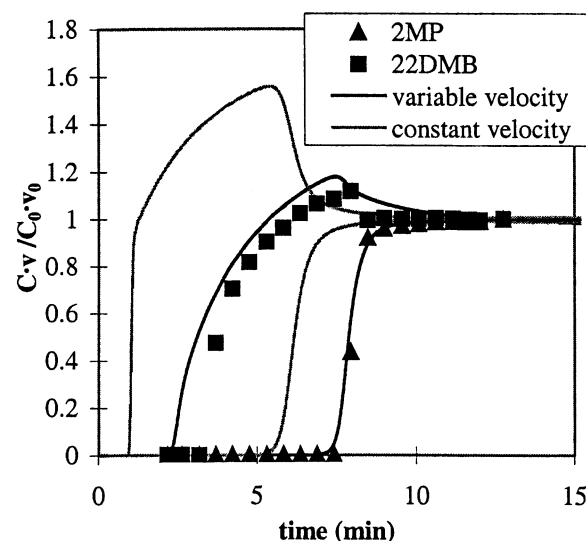Model 1: Maxwell−Stefan with no countercurrent diffusion; model 2: average effective diffusion calculated with Eq. 22; model 3: constant effective diffusion coefficient equal to self-diffusivity.

Figure 9. Simulations of run 13 with different hypotheses.

Model 1: Maxwell−Stefan with no countercurrent diffusion; model 2: average effective diffusion calculated with Eq. 22.

negligible. On the contrary, the two models predict very different breakthrough curves for run 13 (Figure 9). Model 1 is not satisfactory in this case: the breakthrough time predicted with model 2 is much closer to the experimental values. Our conclusion is, therefore, that model 2 is more reliable. Furthermore, due to its simplicity, the time necessary to make a simulation with model 2 is much less. In our case, the Maxwell−Stefan assumption does not allow significant improvement of the simulation results. In addition, it greatly complicates the numerical resolution of the equations. For all these reasons, it was decided to use model 2 for the rest of the simulations.

Influence of Velocity Variations. The velocity variation also implies a lot of numerical complications: for each time interval, global mass variation of the fluid phase has to be integrated over each collocation points along the length of the bed. It is therefore necessary to evaluate the velocity variation amplitude, to make sure that it is really significant. Figure 10 shows the results of the simulations of run 18 with or without velocity variations. It is very clear from this figure that the variation in fluid velocity is very important. If it is not taken into account, the following effects can be seen on the simulated curves:

1. Breakthrough times are smaller, due to the greater average velocity during the run.

Figure 8. Simulations of run 12 with different hypotheses.

Model 1: Maxwell−Stefan with no countercurrent diffusion; model 2: average effective diffusion calculated with Eq. 22.

Figure 10. Simulations of run 18 with model 2: influence of the velocity variations.
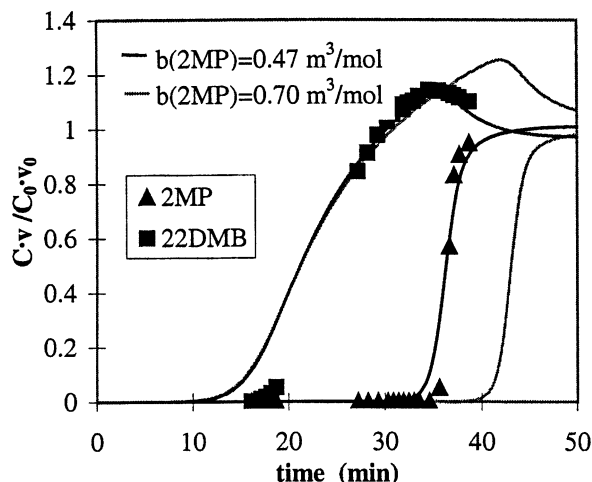
Figure 11. Effect of 2MP Langmuir coefficient on simulated breakthrough curves.

Figure 13. Experiments vs. simulations for run 19: iP, 2MP, and 22DMB breakthrough curves.

2. The roll-up is higher, because the simulated hydrocarbon flow rate depends not only on product concentrations but also on fluid-phase velocity.

Consequently, in our experimental conditions, the velocity variations in the bed are critical and cannot be neglected.

Influence of Parameter Precision. As was said before, the Langmuir parameter b for 2MP varies from 0.47 to 0.7, depending on the concentration range. This means, of course, that the Langmuir model with an adsorption capacity fixed at 4 molecules/cell is not adapted. It was, however, decided to keep the structure of the model, and to fix the value of the Langmuir coefficient for 2MP at a mean value of 0.5 m³/mol. To test the consequence of this approximation of the breakthrough curve, simulations were made with the two extreme values of the Langmuir parameter: 0.47 and 0.7 m³/mol. The results, given on Figure 11, show the great influence that the Langmuir parameter has on the breakthrough time. Therefore, it is very probable that the modeling problem encountered with the 2MP isotherm will produce a nonnegligible uncertainty on the simulated breakthrough curves. This rein-
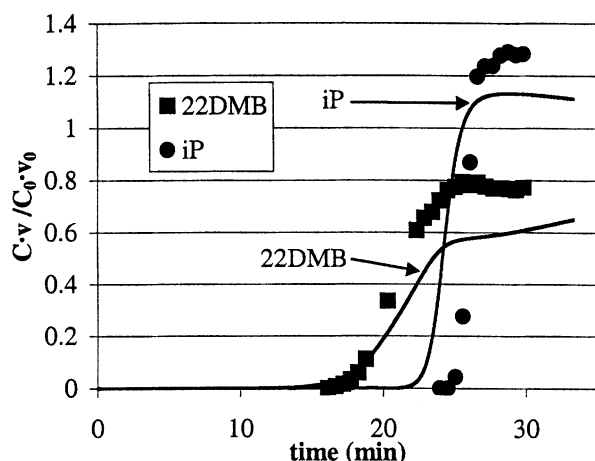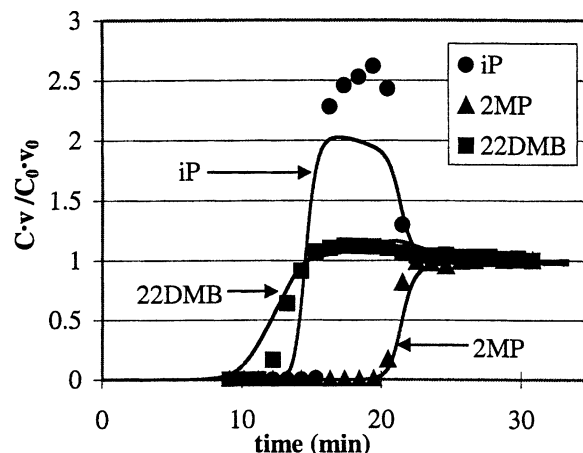
forces our opinion that the Maxwell–Stefan approach is, in our case, too sophisticated in regard to the precision of the more basic parameters.

Simulation Results. All the experiences reported in Table 6 have been simulated, taking the results of the preceding study into account:

- The second diffusion model is used (see Table 7).
- Velocity variation is taken into account.
- The Langmuir parameter for 2MP is fixed at an intermediate value of 0.5 m³/mol.

The results are shown in Figures 12 to 16. The retention times are always in the following order: 2MP > iP > 22DMB. This does not agree with the equilibrium data, which predict the opposite tendency for iP and 22DMB: 22DMB is more adsorbed than iP and should leave the column later. Experiments therefore confirm what was expected: 22DMB diffuses very slowly into the zeolite lattice, which explains why it leaves the column before the monobranched paraffins. The strong roll-up of iP is due to its displacement by the more adsorbed specie 2MP. Simulations represent the experimental breakthrough curves very well, except concerning the binary mix-
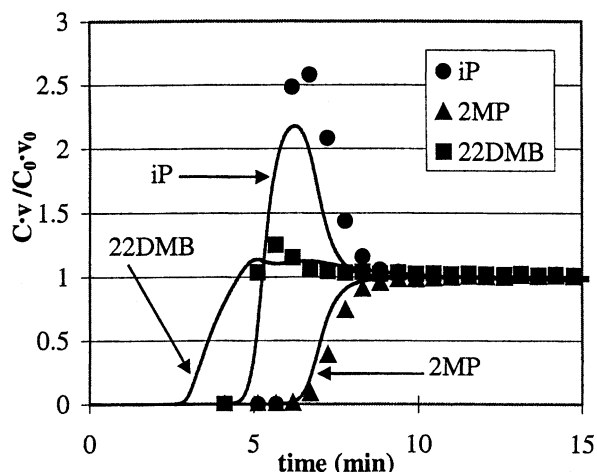

Figure 12. Experiments vs. simulations for run 14: iP and 22DMB breakthrough curves.

Figure 14. Experiments vs. simulations for run 20: iP, 2MP, and 22DMB breakthrough curves.
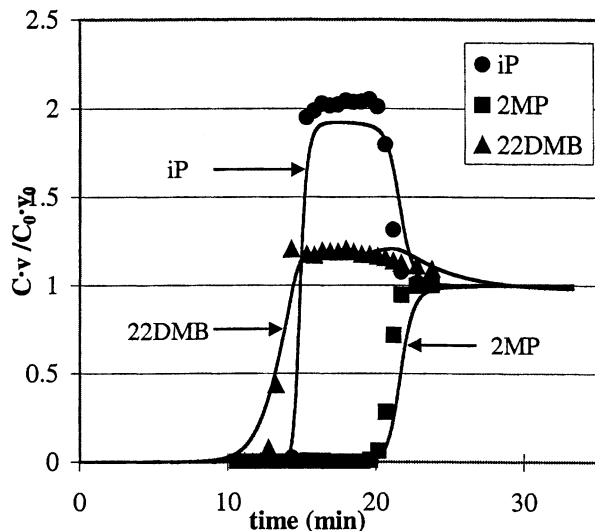
Figure 15. Experiments vs. simulations for run 21: iP, 2MP, and 22DMB breakthrough curves.

tures of iP and 22DMB (Figures 9 and 12). Interactions between iP and 22DMB are very important, and the breakthrough curves of both species depend strongly on the diffusion kinetic of 22DMB. At the beginning of the experiment, iP rapidly enters the lattice of the zeolite. Later, as 22DMB diffuses slowly into the pores, it is pushed out by the less adsorbed molecules of iP. Hence, the retention times of iP and 22DMB depend mainly on the diffusivity of 22DMB and the discrepancy between experimental and simulated results, as this mixture might be due to an inadequate representation of diffusion. It is also possible that the adsorption isotherm for the mixture iP/22DMB is not well represented by the generalized Langmuir model, which uses the same adsorption capacity for both species. In this study, all the parameters are determined from single-component breakthrough curves, and the hypothesis concerning the behavior of the
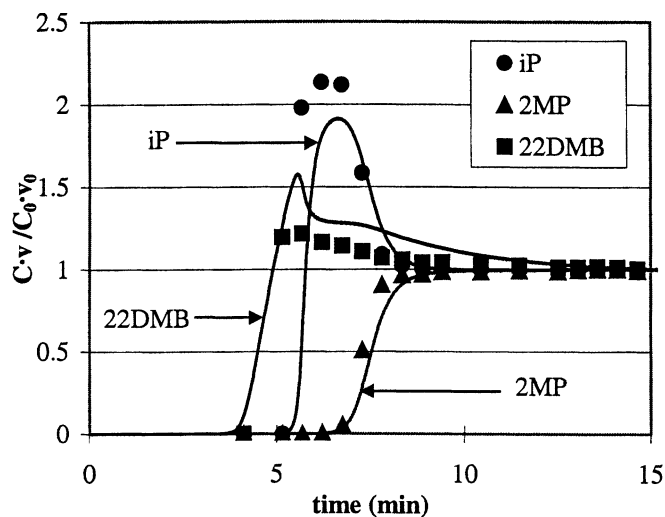

Figure 16. Experiments vs. simulations for run 22: iP, 2MP, and 22DMB breakthrough curves.

mixtures (generalized Langmuir isotherm model, no counter-diffusion coefficients, etc.) may not always be accurate. For ternary mixtures (Figures 13, 14, 15, and 16), this disparity is surprisingly less visible. It is possible that the presence of 2MP reduces the amplitude of the phenomena.

Nevertheless, the model predicts breakthrough curves close to the experimental data, even with a constant Fick diffusion coefficient.

Conclusions

Single-component breakthrough curves of isopentane, 2,2-dimethylbutane and 2-methylpentane in silicalite at 200°C have been measured at different partial pressures. Adsorption isotherms and self-diffusion coefficients have been evaluated for the three paraffins from these curves. Equilibrium data are in good agreement with the results in the literature, except for 22DMB, for which the data dispersion is important.

Multicomponent (binary and ternary) breakthrough curves have also been measured. The limiting diffusion of 22DMB, which is the first to leave the column although it is more adsorbed than isopentane, is clearly visible on these curves.

A model of the bed, including the variation of the effective diffusivity as described by the Maxwell−Stefan equations, has been developed and validated by comparison with the results in the literature. Simulations of the multicomponent breakthrough curves show that:

1. The Maxwell−Stefan approach is not necessary for this system. The accuracy of the simulation is limited by the precision of the equilibrium and diffusion parameters, and it seems inaccurate to enter imprecise parameters into such a sophisticated model.

2. The classic Fick approach with a constant diffusivity (averaged over the whole concentration range with the Darken equation) allows a good representation of our experimental data. The only discrepancy between experimental and simulated results occurs for the binary mixture iP/22DMB. This is attributed to the sensitivity of these breakthrough curves to the adsorption kinetic of 22DMB. This remark points out a contradiction. On the one hand, the diffusion and adsorption of mixtures in zeolite is a very complex phenomenon, and, therefore, requires complex models to be adequately represented. On the other hand, estimation of the parameters to be used in these models is still a challenge. This is true for diffusion coefficients, which can vary over three orders of magnitude, depending on the authors. To a lesser extent, adsorption isotherms can also be difficult to measure, particularly when the diffusion of the molecule is very slow.

3. The ternary (iP, 2MP, and 22DMB) breakthrough curves are well represented with our model. The problem encountered with the iP−22DMB mixture is strongly attenuated. It is, therefore, a very useful tool for the representation and evaluation of multicomponent separation.

Notation

b = "Langmuir" parameter, $m^3 \cdot mol^{-1}$
C = fluid-phase concentration, $mol \cdot m^{-3}$
$\hat{C}$ = vector of C for all components, $mol \cdot m^{-3}$
C_p = macropore concentration, $mol \cdot m^{-3}$
$\hat{C}_p$ = vector of C_p for all components, $mol \cdot m^{-3}$

C_T = global fluid-phase concentration, mol·m^{-3}
D = self-diffusion coefficient, m^2·s^{-1}
D_c = micropore effective diffusivity, m^2·s^{-1}
D_K = Knudsen diffusion coefficient, m^2·s^{-1}
D_L = axial dispersion coefficient, m^2·s^{-1}
D_m = molecular diffusion coefficient, m^2·s^{-1}
D_p = macropore diffusion coefficient, m^2·s^{-1}
d_p = particle mean diameter, m
k_p = mass-transfer coefficient around particles, m·s^{-1}
k_t = mass-transfer coefficient around crystals, m·s^{-1}
L = column length, m
L_p = particle mean length, m
M = molecular weight, g·mol^{-1}
q = adsorbed-phase concentration, mol·m^{-3} or mg·g^{-1}
$\hat{q}$ = vector of q for all components, mol·m^{-3} or mg·g^{-1}
q_s = adsorbed-phase concentration at saturation, mol·m^{-3} or mg·g^{-1}
P = column pressure, Pa
Q = volumetric flow rate, m^3·s^{-1}
R = ideal gas constant, J·mol^{-1}·K^{-1}
R_c = crystals mean radius, m
R_p = particles mean radius, m
r_p = radial particle coordinate, m
r_{pore} = macropore mean radius, m
r_c = radial crystal coordinate, m
T = temperature, K
t = mass ratio of binder in particle
u = superficial velocity, m·s^{-1}
v = interstitial velocity, m·s^{-1}
z = axial column coordinate, m

Greek letters

ϵ_{12} = Lennard−Jones energy, J
ϵ_i = interstitial porosity
ϵ_p = macroporosity
θ = adsorbed-phase fractional saturation $\theta = q/q_s$
θ_t = total adsorbed-phase fractional saturation $\theta_t = \sum_j \theta_j$
μ_f = fluid-phase viscosity, Pa·s
ρ_f = fluid-phase density, kg·m^{-3}
τ = tortuosity factor
σ = characteristic length (Lennard−Jones), Å
Ω^* = diffusion collision integral

Subscripts

0 = at $z = 0$
p = concerning particles
c = concerning crystals

Literature Cited

Cavalcante, C. L., Jr., and D. M. Ruthven, "Adsorption of Branched and Cyclic Paraffins in Silicalite. 1. Equilibrium," *Ind. Eng. Chem. Res.*, **34**, 177 (1995a).

Cavalcante, C. L., Jr., and D. M. Ruthven, "Adsorption of Branched and Cyclic Paraffins in Silicalite. 2. Kinetics," *Ind. Eng. Chem. Res.*, **34**, 185 (1995b).

Farooq, S., and D. M. Ruthven, "Numerical Simulation of a Kinetically Controlled Pressure Swing Adsorption Bulk Separation Process Based on a Diffusion Model," *Chem. Eng. Sci.*, **46**, 2213 (1991).

Farooq, S., M. N. Rathor, and K. Hidajat, "A Predictive Model for a Kinetically Controlled Pressure Swing Adsorption Separation Process," *Chem. Eng. Sci.*, **48**, 4129 (1993).

Jolimaître, E., M. Tayakout-Fayolle, C. Jallut, and K. Ragil, "Determination of Kinetic and Thermodynamic Properties of Branched Paraffins in Silicalite," *Ind. Eng. Chem. Res.*, **40**, 914 (2001).

Kärger, J., and D. M. Ruthven, "Diffusion in Zeolites," *J. Chem. Soc. Faraday Trans. I*, **77**, 1485 (1981).

Kärger, J., and D. M. Ruthven, "On the Comparison Between Macroscopic and n.m.r. Measurements of Intracrystalline Diffusion in Zeolites," *Zeolites*, **9**, 267 (1989).

Millot, B., *Etude du Transport d'Hydrocarbures Saturés dans des Membranes Zéolithiques de Structure MFI*, PhD Thesis, Univ. of Lyon I, Lyon, France (1998).

Millot, B., A. Méthivier, and H. Jobic, "Modelling of Adsorption Equilibria of C4 to C7 Alkanes in MFI type Zeolites," *Proc. Int. Conf. on the Fundamentals of Adsorption*, Giens, France, Elsevier, p. 273 (1998).

Post, M. F. M., J. Van Amstel, and H. W. Kouwenhoven, "Diffusion and Catalytic Reaction of 2-2,dimethylbutane in ZSM-5 Zeolite," *Proc. Int. Zeolite Conf.*, Reno, NV, Guildford, p. 517 (1984).

Reid, R. C., J. M. Prausnitz, and B. E. Poling, *The Properties of Gases and Liquids*, 4th ed., McGraw-Hill, New York (1987).

Ruthven, D. M., *Principles of Adsorption and Adsorption Processes*, Wiley, New York (1984).

Van der Broeke, L. J. P., and R. Krishna, "Experimental Verification of the Maxwell-Stefan Theory for Micropore Diffusion," *Chem. Eng. Sci.*, **50**, 2507 (1995).

Wakao, N., and T. Funazkri, "Effect of Fluid Dispersion Coefficients on Particle-to-Fluid Mass Transfer Coefficients in Packed Beds. Correlation of Sherwood Numbers," *Chem. Eng. Sci.*, **33**, 1375 (1978).

Xiao, J., and J. Wei, "Diffusion Mechanisms of Hydrocarbons in Zeolites: II. Analysis of Experimental Observations," *Chem. Eng. Sci.*, **47**, 1143 (1992).